nature chemistry

ARTICLES

https://doi.org/10.1038/s41557-019-0258-1

Unravelling mechanistic features of organocatalysis with in situ modifications at the secondary sphere

Vasudevan Dhayalan[1,2], Santosh C. Gadekar[1,2], Zayed Alassad[1,2] and Anat Milo[1*]

Secondary-sphere interactions serve a fundamental role in controlling the reactivity and selectivity of organometallic and enzymatic catalysts. However, there is a dearth of studies that explicitly incorporate secondary-sphere modifiers into organocatalytic systems. In this work, we introduce an approach for the in situ systematic modification of organocatalysts in their secondary sphere through dynamic covalent binding under the reaction conditions. As a proof-of-concept, we applied boronic acids as secondary-sphere modifiers of N-heterocyclic carbenes that contained a hydroxy handle. The bound system formed in the reaction mixture catalysed the enantioselective benzoin condensations of a challenging substrate class that contains electron-withdrawing groups. Linear regression coupled with data visualization served to pinpoint the divergent origins of enantioselectivity for different substrates and decision tree algorithms served to formulate selection criteria for the appropriate secondary-sphere modifiers. The combination of this highly modular catalytic approach with machine-learning techniques provided mechanistic insights and guided the streamlined optimization process of a gram-scale reaction at low organocatalyst loading.

Traditionally, optimizing the reactivity and selectivity of catalytic reactions is accomplished by modifying the catalyst structure prior to performing the reaction. Here we propose a method to fine-tune the catalyst structure under reaction conditions by promoting the binding of a modifier to its secondary sphere. The secondary or outer coordination sphere was first described more than a century ago by Alfred Werner in the context of organometallic complexes as groups that are not directly bonded to a metal, but are rather coordinated to the ligands[1–3]. This definition has since been expanded to any moiety in the molecular microenvironment of coordination compounds that influences the orientation and electronic properties of their ligands by introducing non-covalent interactions, such as hydrogen bonding, electrostatic forces and hydrophobic effects[4–6]. Although it is now well established that such interactions have a fundamental effect on the reactivity and selectivity in enzymatic catalysis[7–9], metal-mediated processes and transition metal chemistry[4–6,10–14], the systematic study of secondary-sphere interactions in organocatalysis remains uncommon. The secondary sphere comprises moieties that are not an integral part of an active site, yet are located in proximity to it and are involved in its mechanism of action through dynamic or non-covalent interactions. These interactions control the geometry and electronic properties of the reaction intermediates and transition state(s). In this work, we establish a straightforward and systematic strategy to modify the secondary sphere of organocatalysts by combining a highly modular catalytic system with mathematical modelling techniques to facilitate the discovery and prediction of secondary-sphere design principles. This methodology is predicated on modifying the structure of an organocatalyst in situ under reaction conditions and providing a tunable handle for the nuanced recognition of substrates by their geometry and electronic properties, and thus streamline the optimization, mechanistic study and discovery of organocatalytic systems.

By promoting the in situ binding of a modifier to the catalytic system under reaction conditions, we intended to curtail the need for prior synthetic steps to fine-tune catalytic scaffolds. The binding mode of the modifier was required to be orthogonal to catalytic activity to avoid catalyst inhibition. Likewise, the modifier was to be located in close proximity to the active site and possess the capacity for dynamic and non-covalent interactions that could guide reactivity and selectivity. To achieve this goal, we selected to harness the propensity of aryl boronic acids (BAs) to form boronic ester bonds with hydroxyl groups (Fig. 1a). The practical benefit of this binding mode stems from the availability and structural diversity of BAs and the ease of identifying and preparing organocatalysts with pendant hydroxyl groups. Boronic ester bonds can be described as dynamic covalent bonds, which are considered to have a dual nature, because—depending on the conditions (solvent, temperature, pK_a, additives)—they can undergo rapid exchange, similar to a non-covalent bond, or exhibit stability, similar to a covalent bond. Whereas the application of dynamic covalent chemistry has flourished in the fields of supramolecular and materials chemistry, it has been limited in organocatalysis[15–27]. We hypothesized that BAs would bind to the catalyst under reaction conditions and affect its reactivity and selectivity by promoting dynamic covalent and non-covalent π and hydrogen bonding interactions with the substrates at the different steps of the catalytic cycle. Concomitantly, the application of mathematical modelling, coupled with mechanistic experiments, would uncover the guiding principles by which BAs influence catalysis.

As a proof-of-concept, we sought to identify a known organocatalytic system in which a hydroxyl group was located in proximity to the active site and was explicitly invoked to explain the reactivity and selectivity. Such a system was reported by Zeitler, Connon and co-workers in the context of the benzoin condensation ($\mathbf{Cat_{5F}}$ (Fig. 1b))[28,29]. The benzoin condensation has been studied for over a century and involves the coupling of two aldehydes to afford a benzoin product through the inversion of polarity (umpolung) of one of the two aldehydes (Fig. 1c shows the commonly accepted catalytic cycle). This reaction is influenced by non-covalent interactions[30–32] and, indeed, the organocatalytic system described by Zeitler and Connon was considered the most efficient in terms of

[1]Department of Chemistry, Ben-Gurion University of the Negev, Beer Sheva, Israel. [2]These authors contributed equally: Vasudevan Dhayalan, Santosh C. Gadekar, Zayed Alassad *e-mail: anatmilo@bgu.ac.il

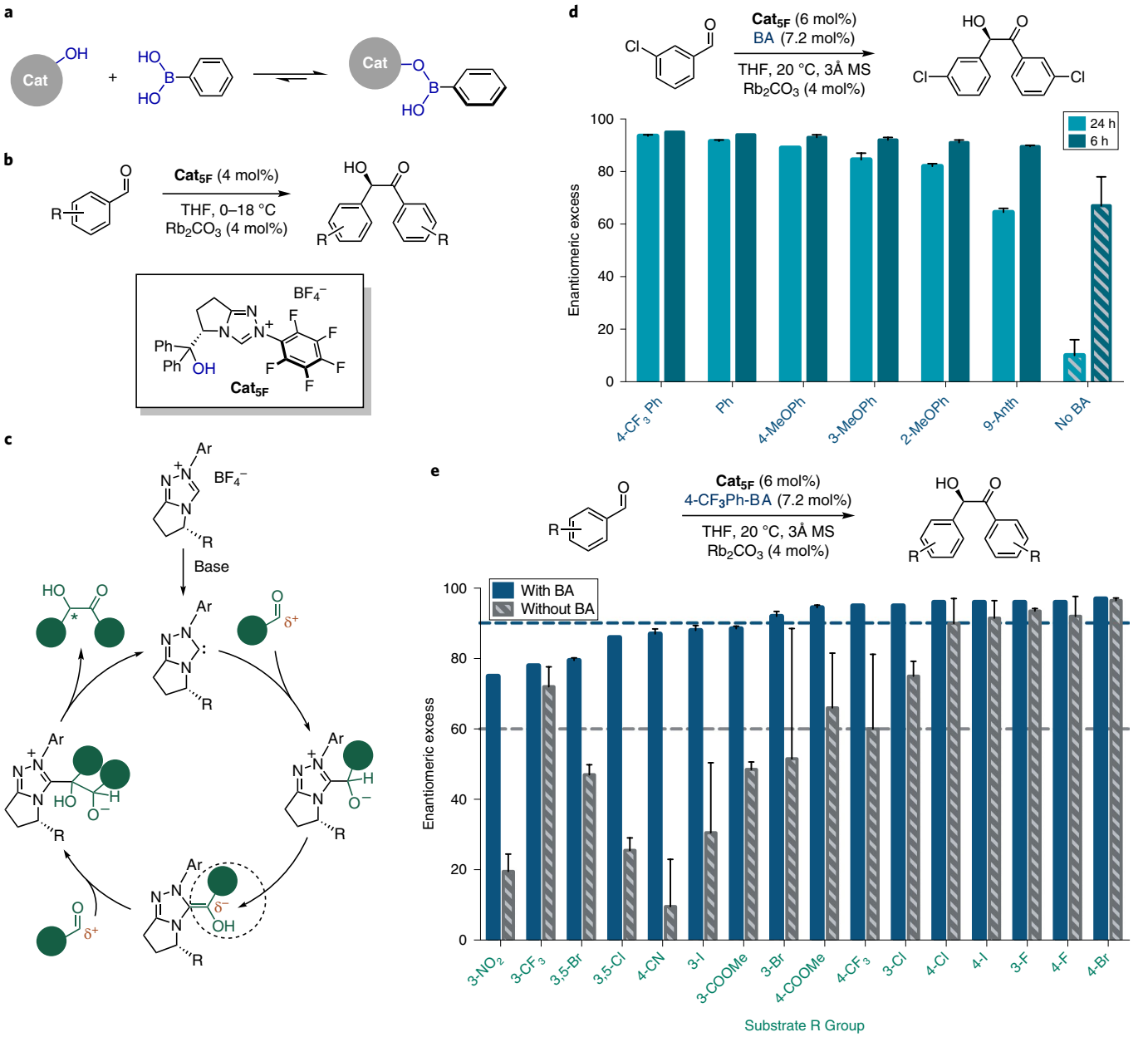

Fig. 1 | The influence of secondary-sphere modulation of NHCs on the benzoin reaction. a, Conceptual framework: stabilizing boronic ester bonds in situ under catalytically relevant conditions to tune the reactivity and selectivity at the secondary sphere. **b**, The optimal organocatalyst for the benzoin reaction to date developed by Zeitler, Connon and co-workers contains a hydroxyl group invoked in non-covalent interactions and is limited in its scope of substrates with electron-withdrawing groups[28]. **c**, Commonly accepted catalytic cycle for the benzoin condensation. **d**, Comparison of the enantioselectivity obtained in the benzoin condensation using several BA modifiers and 3-chlorobenzaldehyde as the substrate at 6 hours and at 24 hours. Error bars represent the range of two measurements. 9-Anth, 9, anthracene. **e**, Comparison of the enantioselectivity obtained in the benzoin condensation with different electron-withdrawing substituents in the presence and absence of 4-CF_3Ph-BA. Dashed horizontal lines represent the average enantioselectivity across each set: 90% e.e. (e.r. 95:5) with 4-CF_3Ph-BA and 60% e.e. (e.r. 80:20) in its absence. Reactions were run for 6 hours. Error bars represent the s.d. between at least two measurements.

catalyst loading and selectivity to date[33]. Nonetheless, the paucity of examples of organocatalytic enantioselective benzoin condensations of aldehydes with electron-withdrawing substituents provided an ideal opportunity to examine the concept of leveraging secondary-sphere interactions by the in situ introduction of BAs.

Results and discussion

Catalytic experiments. Reactions were performed with a model substrate, 3-chlorobenzaldehyde, reported by Zeitler, Connon and co-workers to afford an enantiomeric ratio (e.r.) of 84:16. Reactions that were conducted for 24 h with different BAs led to a range of enantioselectivity values up to 97:3 (Fig. 1d). To our surprise, the full set of BAs studied led to e.r. values above 95:5 for 6 h reactions. Consequently, we set out to study a scope of electron-withdrawing substrates in the presence of the best performing BA, 4-(trifluoromethyl)phenylboronic acid (4-CF_3Ph-BA). The e.r. obtained for the substrates in the presence of 4-CF_3Ph-BA was between 88:12 and 98.5:1.5 and was consistently improved and more reproducible compared to the same reaction in the absence of BA (Fig. 1e).

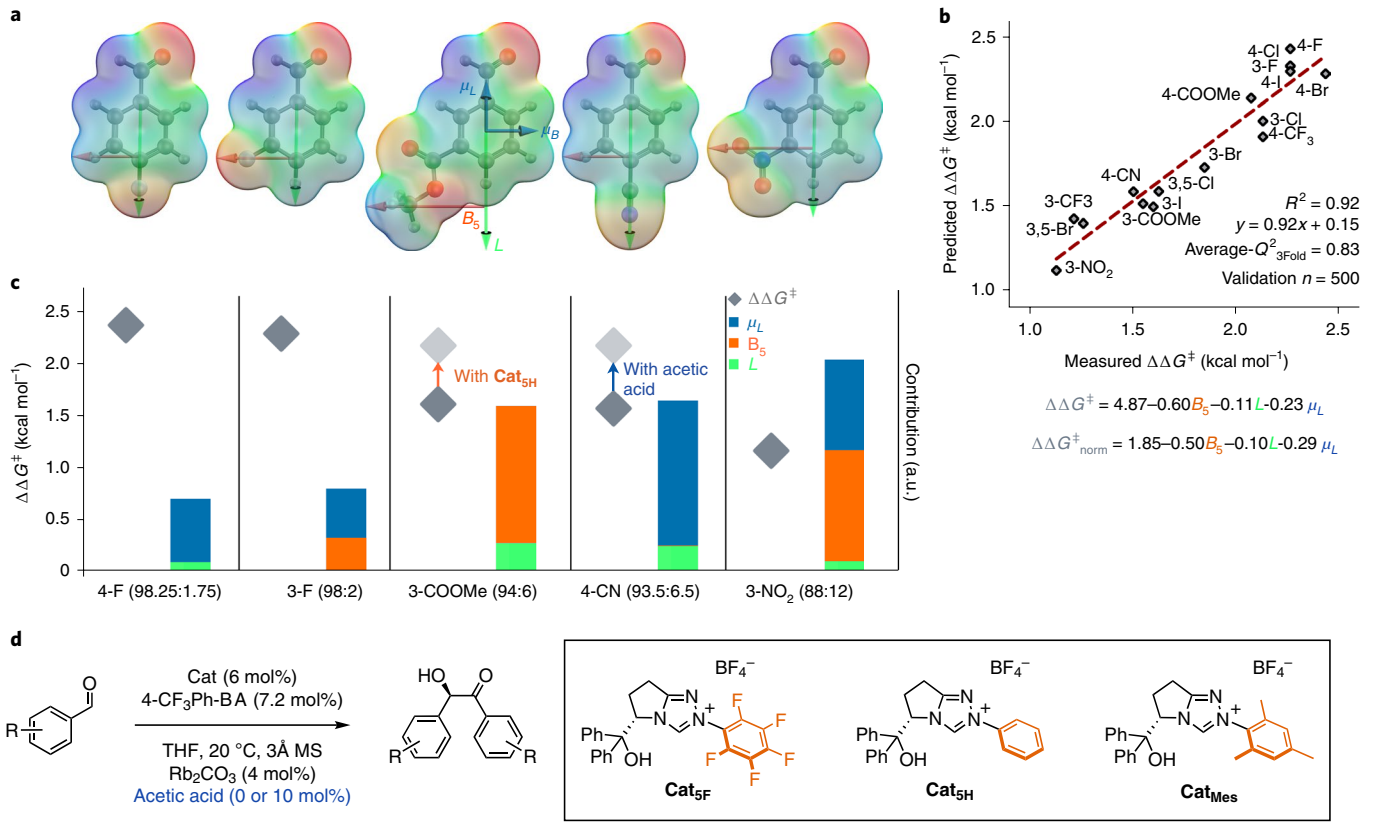

Fig. 2 | Multivariate model of the enantioselectivity for 6 hour reactions across a set of electron-withdrawing aldehydes. a, Parameters that were identified as predictive for the enantioselectivity in this reaction. **b**, Measured versus predicted enantioselectivity represented as $\Delta\Delta G^{\ddagger} = -RT\ln([R]/[S])$ given by a model that included three molecular descriptors (the normalized parameters were obtained by subtracting the mean and dividing by the s.d.). Goodness-of-fit is represented by R^2 and the average Q^2 of a threefold (Q^2_{3fold}) validation performed 500 times on randomized sets. **c**, Graphical representation of the relative contribution of each parameter to the predicted enantioselectivity (grey diamonds) that highlights an inverse correlation of all three parameters with the resulting enantioselectivity and the putative differences in the origin of enantioselectivity for different substrates. Light grey diamonds represent the enantioselectivity on the addition of either acetic acid (blue arrow) or **Cat$_{5H}$** (orange arrow). **d**. Conditions and different catalysts tested in the reaction.

Substrate trend analysis for 6 hour reactions. The obtained results did not follow a simple electronic or steric trend (Fig. 1e). Therefore, we sought to identify a multivariate model to shed light on the origin of enantioselectivity in the presence of 4-CF$_3$Ph-BA. The substrate was the only reaction component that changed between experiments and, therefore, molecular descriptors that pertained to the geometric, steric and electronic features of the substrates were collected. Hammett values[34], Sterimol parameters[35], vibration frequencies and intensities[36], and NBO charges[37] were evaluated. As the models obtained with these known parameters were not satisfactory in terms of their goodness-of-fit (Supplementary Section 5 gives details and several examples), we decided to add the components of the dipole moment using a fixed Cartesian coordinate system across all substrates (Fig. 2a). It was hypothesized that this new parameter system would be advantageous to describe the directional electrostatic and electronic effects. Indeed, with the introduction of the dipole moment components, a highly predictive model was identified (Fig. 2b). The model included the component of the dipole moment on the L (maximal length) axis (μ_L) and two steric Sterimol parameters, the maximal length of the aldehyde ring with its substituents (L) and the maximal width perpendicular to the length (B_5 (Fig. 2a)). To better understand the meaning of these parameters, a graphical representation of each parameter's contribution to the predicted enantioselectivity was produced by applying the model to the respective parameters for several of the substrates (Fig. 2c; Supplementary Table 7 gives further details). By doing so we were in the position to probe experimentally the underlying factors that regulate the enantioselectivity each parameter signifies. The juxtaposition of parameter contributions and $\Delta\Delta G^{\ddagger}$ values highlights the inverse correlation between each of these parameters and the resultant enantioselectivity. Namely, the e.r. was diminished for substrates that were longer, wider and had a strong dipole on the L axis.

To interrogate the role of each parameter in predicting enantioselectivity, we focused on two substrates that afford similar e.r. values, but for which different parameters predominantly predict the selectivity, 3-carbomethoxybenzaldehyde and 4-cyanobenzaldehyde (Fig. 2c). As μ_L is aligned with the aldehyde moiety it was speculated that it could represent the directional electron-withdrawing capacity of the substituents on the benzoin product and, therefore, could be related to base-catalysed racemization. To probe this assumption further, correlations between μ_L and the other parameters were sought and, indeed, a strong correlation emerged between the dipole moment on the length axis and the charges on the aldehyde moiety (Supplementary Fig. 17 gives details). To mitigate the postulated effect of the base, catalytic reactions with each of the substrates in the presence of 10 mol% of acetic acid were performed. It was anticipated that if the dipole moment is related to base-catalysed racemization, the addition of acetic acid would have a greater influence on 4-cyanobenzaldehyde because μ_L is the main parameter that predicts its enantioselectivity (Fig. 2c, blue). Indeed, following our prediction, with the addition of acetic acid, the $\Delta\Delta G^{\ddagger}$ value

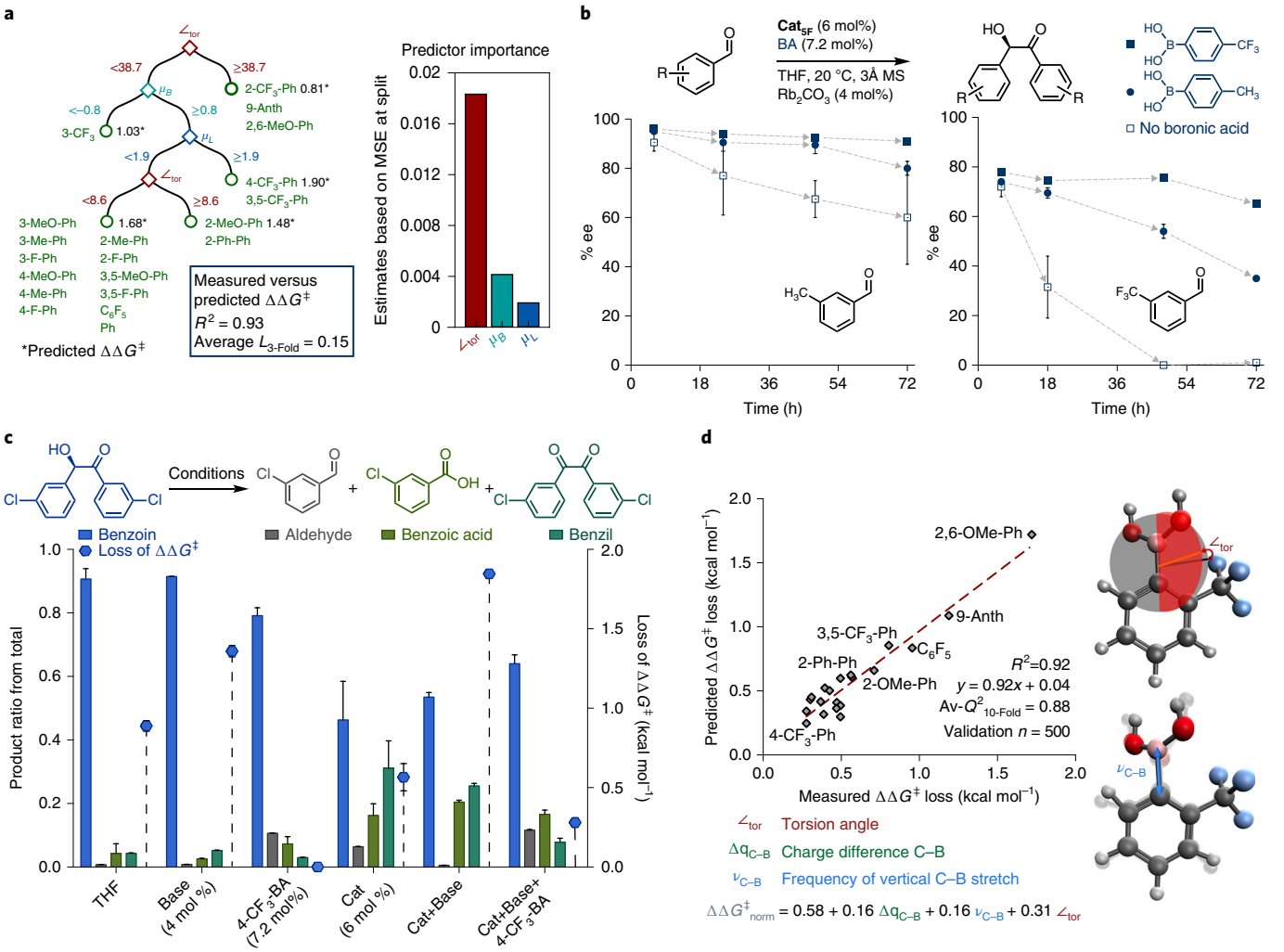

Fig. 3 | Disentangling the effect of racemization. a, Model for 24 hour reactions with 3-chlorobenzaldehyde as the substrate and different BAs: decision tree (left (see text)) and estimation of each predictor's importance based on the mean standard error (MSE) decrease at each node (right). Bold black numbers are the predicted $\Delta\Delta G^{\ddagger}$(in kcal mol^{-1}). Goodness-of-fit is represented by R^2 and the average L_{3fold} (predictive loss) value of a threefold validation performed 500 times on randomized sets. $\angle_{tor}$, torsion angle. **b**, Erosion of enantioselectivity over time with and without BAs for electron-donating and withdrawing substrates 3-methylbenzaldehyde and 3-trifluoromethylbenzaldehyde. Error bars represent the range of two measurements. **c**, Racemization experiments starting from enantioenriched 3-chlorobenzoin: the left axis represents product distribution ratios and the right axis represents the loss of enantioenrichment in $\Delta\Delta G^{\ddagger}$. Error bars represent the s.d. between at least two measurements. **d**. Linear regression model and structural features for loss of enantioenrichment in racemization experiments of enantioenriched 3-chlorobenzoin with different BAs. ν_{C-B}, charge difference C–B; q_{C-B}, frequency of vertical C–B stretch.

for 3-carbomethoxybenzaldehyde remained 1.6 kcal mol^{-1}, whereas for 4-cyanobenzaldehyde it increased from 1.55 to 2.02 kcal mol^{-1} (Fig. 2c, blue arrow). We suspected that the maximal width, B_5, may be related to electrostatic effects given that such effects were found computationally to have a strong influence on enantioselectivity in N-heterocyclic carbene (NHC) catalysis[38]. Based on the assumption that the substituents on the catalyst aryl ring would have a decisive influence on the electrostatic interactions, the reaction of each of these two substrates was performed using two different catalysts (**Cat$_{5H}$** and **Cat$_{Mes}$** (Supplementary Section 6.2)). It was anticipated that if the maximal width is representative of the electrostatic interactions with the catalyst, we would see a greater effect on 3-carbomethoxybenzaldehyde because B_5 is the main parameter that predicts its enantioselectivity (Fig. 2c, orange). In accord with our predictions, for 3-carbomethoxybenzaldehyde the $\Delta\Delta G^{\ddagger}$ increased to 2.02 kcal mol^{-1} (Fig. 2c, orange arrow) in the presence of **Cat$_{5H}$**, whereas for 4-cyanobenzaldehyde it did not change significantly. **Cat$_{5H}$** has an increased pK_a value compared to **Cat$_{5F}$**, and thus one could consider this to be the origin of its increased enantioselectivity[28,39,40]. However, if this were the case, **Cat$_{Mes}$**, which is estimated to have a greater pK_a value[39,40], would be expected to increase enantioselectivity further, but in fact it significantly decreases it (Supplementary Table 13). This outcome fits well with electrostatic interactions, which would presumably be disrupted due to the steric hindrance and torsional constraints introduced by a mesityl ring. Overall, these results highlight the unique capacity of multivariate modelling and data visualization approaches to distinguish the origins of enantioselectivity for different substrates even when their e.r. value is similar. As demonstrated, such insights can facilitate the tailored optimization of reaction outcomes.

BA trend analysis for 24 h reactions. Due to the erosion in enantioselectivity during 24 h reactions and the observation that adding acetic acid improved the enantioselectivity for certain substrates, it

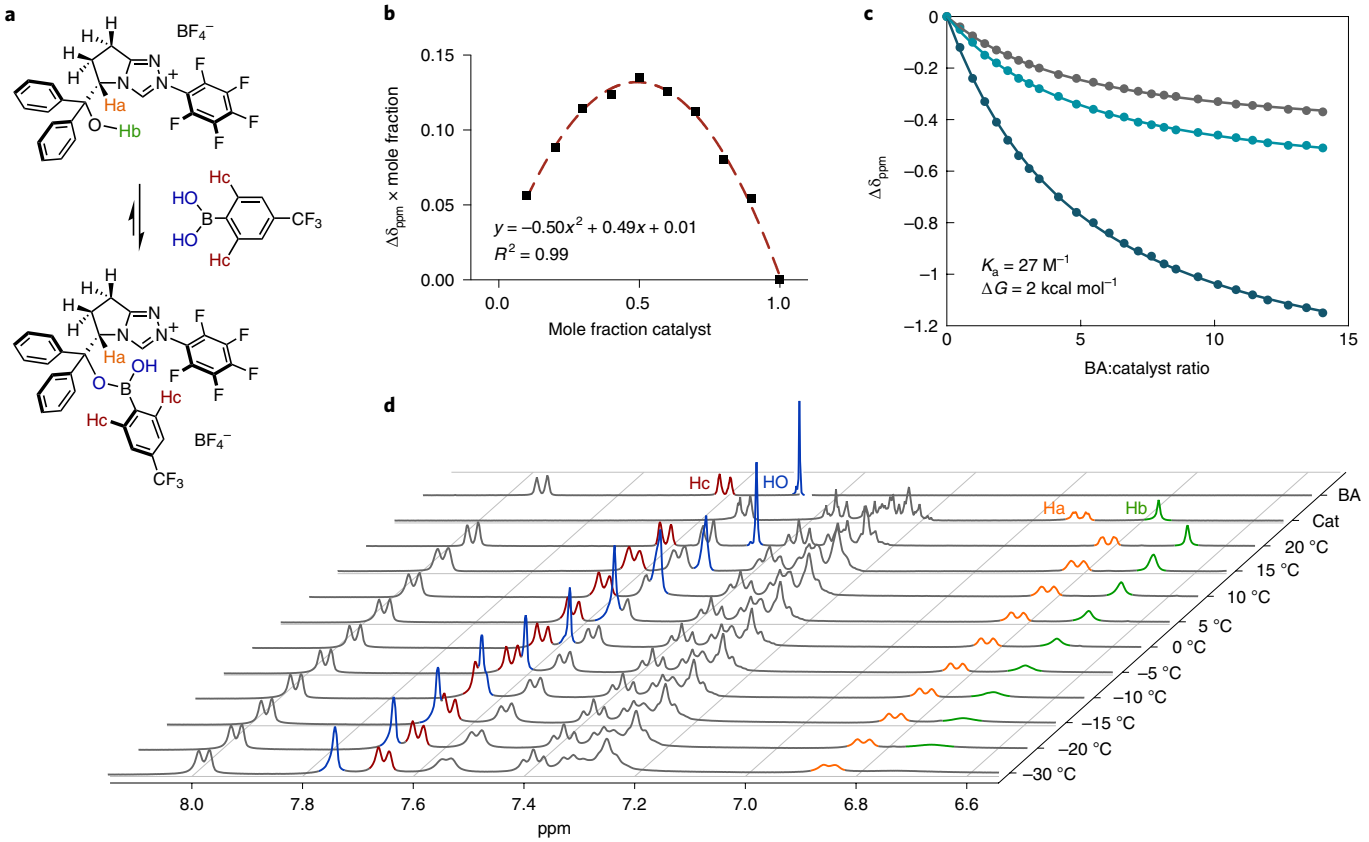

Fig. 4 | Binding studies of BA to NHC in THF. a, Proposed dynamic covalent binding. **b**, Job's plot reveals a 1:1 binding stoichiometry. **c**, NMR binding studies using a global fit of three proton peak shifts (Supplementary Section 3.2 gives details). **d**, NMR at lower temperatures reveals slower exchange rates and stabilization of the boronic ester.

seemed likely that the 24 h reaction results represent two processes: benzoin product formation and subsequent racemization. As the outcome was a result of these two competing processes, we were unable to identify a model to describe the 24 h reactions by linear regression. We turned to decision tree analysis and were able to identify a model that highlighted the BA structural features related to the determination of selectivity at 24 h reactions (Fig. 3a). Regression trees resemble flow charts, in which each node (diamond) represents an attribute, each branch represents the splitting criteria of this attribute (on the left the values below the split and on the right those equal to or above it) and each leaf, or terminal node (green circle), contains a class of BAs (green) that lead to a predicted value, in our case the obtained $\Delta\Delta G^{\ddagger}$ (black). The top node in a tree is the root node, which in this case is the dihedral or torsion angle. BAs that bear a relatively high torsion angle between the BA moiety and the aromatic residue lead to the lowest enantiomeric excess at 24 h, predicted at 0.81 kcal mol^{-1}. The component of the dipole moment in the direction of the width (μ_B) serves to distinguish 3-CF_3Ph-BA, which has a relatively large electron-withdrawing group on the *B* axis and is predicted to give $\Delta\Delta G^{\ddagger} = 1.03$ kcal mol^{-1}. The component of the dipole moment in the direction of the length (μ_L) classifies the BAs with the highest enantioselectivity, predicted at 1.9 kcal mol^{-1}, which contains the largest electron-withdrawing groups on the *L* axis, 4-CF_3 and 3,5-CF_3. Finally, an additional limitation on the torsion angle separates the remaining BAs with longer 2-substituent groups, 2-MeO and 2-Ph, from the rest of the set.

We sought to probe whether the racemization process over long reactions was unique to electron-withdrawing substrates by following the reaction over time for 3-methyl- and 3-trifluoromethylbenzaldehyde (Fig. 3b). In both cases, in the absence of BA the initial enantioselectivity decreased over time and the reproducibility of the results was limited[41]. Adding 4-MePh-BA or 4-CF_3Ph-BA led to an improved stability of enantioselectivity over time and the latter shows a superior performance over longer periods of time, which is especially notable in the presence of electron-withdrawing substrates.

Racemization analysis. Although the decision tree model serves to classify BAs based on their structural features and is predictive of the observed enantioselectivity at 24 h, it is limited in terms of delineating the racemization mechanism. To probe the mechanistic underpinnings of the racemization process, several control experiments were designed in which enantioenriched 3-chlorobenzoin was subjected to reaction conditions while omitting certain components. The erosion of enantiomeric excess and the product distribution were analysed by HPLC (Fig. 3c and Supplementary Section 6.6). From these results, it appears that BA suppresses both the base- and NHC-catalysed racemization processes as well as the oxidation process to benzil. The reversibility of the benzoin condensation has previously been described in the literature[42–44], and the accretion of aldehyde in the presence of BA suggests that it may be involved in the retro-benzoin process. Overall, these results suggest that BAs are probably involved in both the selectivity- and turnover-determining steps of the benzoin reaction. This assertion was supported by the exceedingly different reaction progress profiles that emerged by following the change in product yield over time in the presence and absence of BA (Supplementary Table 25).

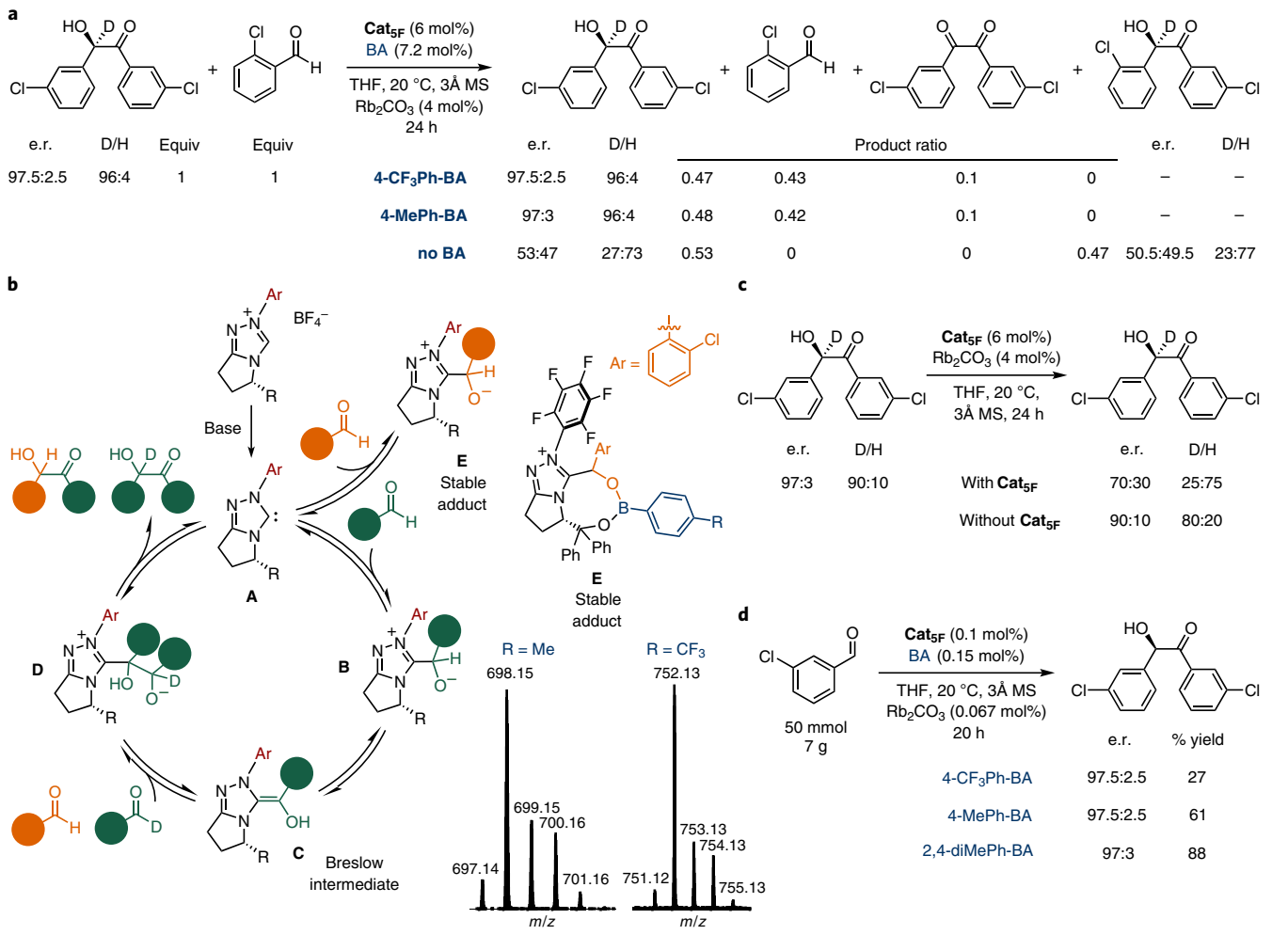

Fig. 5 | Cross-over experiments between the benzoin product and an additional aldehyde. a, Enantioenriched and deuterated 3-chlorobenzoin and 2-chlorobenzaldehyde under reaction conditions with and without BAs. The enantioenrichment and deuterium incorporation were determined for the remaining 3-chlorobenzoin and for the cross-benzoin product. Complete erosion of enantioenrichment and substantial deuterium scrambling reveal the full reversibility of the reaction in the absence of BA. **b**, Proposed catalytic cycle and the formation of a stable acyl anion adduct with 2-chlorobenzaldehyde, which is presumed to be further stabilized by BA. Mass spectrometry (matrix-assisted laser desorption/ionization–time of flight) is consistent with the formation of a stabilized 1:1:1 adduct of NHC:BA:2-chlorobenzaldehyde. One plausible stable adduct that fits with the observed *m/z* is proposed. **c**. Racemization and deuterium-loss experiments (24 hours) in the presence of base with and without the NHC catalyst reveal that the erosion of enantioenrichment and the loss of the deuterium label under reaction conditions are enhanced by the presence of the NHC catalyst. **d**. Streamlined optimization of a gram-scale reaction at a 0.1 mol% NHC loading with different BAs.

To probe the influence of changes to the structure of BA on the racemization process we ran 24 h racemization reactions with different BAs (Supplementary Section 6.5). We were able to identify a highly predictive model that reflected the structural features leading to racemization (Fig. 3d). Akin to the model for 24 h reactions, the torsion angle was key and BAs with minimal torsion angles led to a decreased racemization. In addition, several features that related to the BA moiety were implicated in describing the observed racemization. Enhanced racemization was observed using BAs with higher C–B vibration frequencies and larger differences in charge between the boron and the adjacent carbon on the aromatic moiety. Increased charge differences and higher vibration frequencies entail a relative negative charge on carbon, which decreases the electrophilicity of boron, thus decreasing its affinity to sequester the base. However, a less-electrophilic boron would also be less likely to bind to a hydroxy group on the NHC catalyst or any hydroxy-containing intermediate on or off the catalytic cycle. This option would incur a higher steric penalty, and thus could be reflected by the decrease in selectivity observed at increased torsion angles. Note that the results from 24 h reactions and racemizations are not correlated and only the racemization results are somewhat correlated to the pK_a of the BAs (Supplementary Figs. 21–23). Taken together with the more pronounced importance of the torsion angle in predicting 24 h reactions, we hypothesize that beyond decelerating base catalysed racemization, BAs are involved in inhibiting the retro-benzoin reaction by binding to NHC or one of its reactive intermediates.

Binding studies. The binding between BA and **Cat$_{5F}$** was studied by NMR (Supplementary Section 3 gives experimental details). A Job plot was obtained in THF-d_8 that suggests that BA and **Cat$_{5F}$** afford a 1:1 complex (Fig. 4a,b)[45]. A 1:1 binding constant of 27 M^{-1} was calculated based on fast exchange equilibria on the NMR timescale, which corresponds to 2 kcal mol^{-1} (Fig. 4c)[46]. Based on these results, the weakly bound **Cat$_{5F}$**–BA complex could be hydrogen bonded or could involve the release of a water molecule to form a dynamic boronic ester bond (Fig. 4b). To study these possibilities, variable temperature ^{1}H NMR measurements were performed in THF-d_8. At room temperature, both the proton on the stereogenic centre, Ha

(orange, Fig. 4d), and the hydroxyl peak of the $\mathbf{Cat}_{5F}$, Hb (green, Fig. 4d), shifted upfield by 0.1 ppm on the introduction of BA, which rules out hydrogen bonding as we would expect the BA hydroxylic proton (blue, Fig. 4d) to be shifted as well. BAs have been shown to form dynamic-covalent bonds with hydroxy groups[47], therefore, a fast exchange on the NMR scale was hypothesized between a bound boronic ester and the free $\mathbf{Cat}_{5F}$ and BA. To test this proposal, low-temperature NMR measurements were performed. With the decrease in temperature, the $\mathbf{Cat}_{5F}$ hydroxyl peak, Hb (green), broadened and decreased in intensity, the BA hydroxyl peak, OH (blue), shifted downfield, as did the protons at the *ortho* positions, Hc (red) (Fig. 4d). These results fit well with the stabilization of the proposed boronic ester at lower temperatures. Note that under the reaction conditions base and molecular sieves were added, which are both known to promote the formation of boronic esters[47–49].

Cross-over experiments with isotopic substitution. The non-homogeneous reaction conditions are limiting for kinetic studies, so cross-over reactions of deuterated 3-chlorobenzoin with 2-chlorobenzaldehyde were performed to test the influence of BAs on the different steps in the proposed catalytic cycle (Fig. 5a). 2-chlorobenzaldehyde was selected because it was found to form stable and less-reactive acyl anion adducts[50], and therefore it was hypothesized that this experiment would produce predominantly one cross-over product (Fig. 5a). Indeed, in the absence of BA, the reaction led to an equivalent amount of 3-chlorobenzoin and one cross-over benzoin isomer, both with negligible enantioenrichment. The 3-chlorobenzoin deuterium incorporation loss was significant and a slight deuterium uptake was observed for the cross-over product (Supplementary Table 33 gives details). Based on our control experiments (Fig. 3c), it was postulated that the racemization and deuterium loss could arise from both the reversibility of the benzoin reaction and a base-catalysed process (Fig. 5b). To distinguish between these two options, additional racemization control experiments were performed in which deuterated 3-chlorobenzoin was subjected to reaction conditions in the absence of BA with and without the NHC catalyst (Fig. 5c and Supplementary Table 36). The enantioenrichment and deuterium loss was much more significant in the presence of the NHC catalyst. This result supports the hypothesis that a major amount of deuterium loss stems from the complete reversibility of the benzoin reaction to release a protonated aldehyde, which can then undergo a nucleophilic attack by another Breslow intermediate (Fig. 5b). To our surprise, in the presence of BA no cross-over, deuterium loss or enantioenrichment loss were observed (Fig. 5a). In combination with the racemization experiments, these results shed light on the role of BA in mitigating racemization. We hypothesize that BA increases the energetic barrier for the release of the protonated aldehyde in the presence of NHC, probably by binding to the reactive intermediates and transition states under the reaction conditions. As the 2-chlorobenzaldehyde forms stable acyl anion adducts and the BA is presumed to increase the barrier for the release of the aldehyde, it was expected that an extremely stable acyl anion adduct could be formed in the presence of BA. Accordingly, mass spectrometry analysis (matrix-assisted laser desorption/ionization–time of flight) was consistent with the formation of a stable 1:1:1 NHC:BA:2-chlorobenzaldehyde adduct in the presence of two different BAs (Fig. 5b). These results strongly suggest that BAs are not only involved in regulating the selectivity and mitigating the base and NHC-induced racemization, but also take part in the turnover determining step(s) of this reaction by binding to NHC and its reactive intermediates. In addition, experiments with a catalyst that does not contain a hydroxy group were performed and support our hypothesis that this is not merely cooperative catalysis, but rather a modification at the secondary sphere (Supplementary Section 6.11). We are currently conducting density functional theory and kinetic studies to further investigate the mechanism and mode of BA binding throughout the catalytic cycle, and the precise origin of reactivity and selectivity.

Gram-scale reactions. Based on the insight gained through the mechanistic studies of this system, we wished to exploit the stabilization afforded by BAs to perform a gram-scale reaction at a low catalyst loading (Fig. 5d). The reaction was performed at a 50 mmol scale (7 g) with a catalyst loading of 0.1 mol%, with 0.15 mol% BA and 0.067 mol% base. Such mild conditions and low catalyst loading are unprecedented for the benzoin condensation with an NHC catalyst. We started by applying 4-CF_3Ph-BA and, although the e.r. was 97.5:2.5, the yield even after 72 h was only 34% (Supplementary Section 6.14). It was noted that under these benign conditions, racemization over time was negligible. We turned to additional BAs that led to the least loss of enantioselectivity in the 24 h reactions, and of these we opted for electron-donating BAs with the assumption that they may afford higher turnover frequencies based on their increased yields (Supplementary Table 15). This left us with the BAs on the lower left node of the regression tree predicted at $\Delta\Delta G^{\ddagger} = 1.68$ kcal mol^{-1}. We selected 4-MePh-BA and, indeed, the e.r. at 20 h was also 97.5:2.5, but the yield increased to 60%. Finally, we hypothesized that an additional 2-Me group would (1) not influence the torsion of the BA and (2) not significantly increase the dipole moment in the direction of L or B_5, and thus should not erode enantioselectivity. Yet, we expected an increase in the yield due to the addition of an electron-donating group. Therefore, the reaction was run with 2,4-diMePh-BA, which led to an e.r. of 97:3 and a yield of 88% after 20 h.

Based on the premise that dynamic covalent binding with BAs could serve to modify the secondary sphere of organocatalysts, we selected a system in which such interactions could be envisioned near a catalytic site. As a proof-of-concept, we were able to regulate the reproducibility and improve the selectivity of the benzoin condensation for a challenging substrate class that contained electron-withdrawing groups. Furthermore, the development of a machine-learning-based decision tree for the BA selection streamlined the optimization of a gram-scale benzoin reaction with the lowest catalyst and base loading to date using an NHC organocatalyst. We propose that the approach developed in this work could be applied to systematically modify and regulate the secondary sphere of numerous organocatalytic systems to give an increased stability and reproducibility, an industrially relevant catalyst loading and a tunable handle for controlling both reactivity and selectivity.

Methods

General experimental procedure for 6 and 24 h benzoin reactions in the presence of BAs. Enantioselective benzoin reactions were run in 8 ml vials with screw-cap septa and stirred at 500 revolutions per minute (r.p.m.). A dry, argon-flushed 8 ml vial equipped with a magnetic stir bar was charged with Rb_2CO_3 (0.045 mmol) and a 3 Å molecular sieve (MS) (50 mg) and dried at 200 °C in the oven overnight. The vial was then heated with a heat gun under an argon flow for 5 min and cooled to room temperature. The NHC catalyst (0.066 mmol) and aryl BA (0.079 mmol) were added and flushed with argon followed by the addition of 1 ml of anhydrous THF. The reagents were allowed to stir for 10 min at 20 °C under an argon atmosphere and then arylaldehyde (1.1 mmol) was added. The reaction mixture was stirred at 20 °C for 6 or 24 h. The reaction was quenched with distilled acetic acid (30 µl, 0.48 mmol) and stirred for 10 min. The solvent was removed under a nitrogen flow. To calculate the NMR yields, a stock solution of 1,3,5-triisopropylbenzene (1 mmol) in $CHCl_3$ (10 ml) was prepared and each reaction mixture was dissolved in 1 ml of the stock solution. An aliquot of the dissolved reaction mixture (200 µl) was used for HPLC enantioenrichment analysis by filtering through silica gel (500 mg) and then washing with $CHCl_3$ (5 × 2 ml). After evaporating the solvent in vacuo, the crude product was dissolved in isopropyl alcohol and the sample was ready for HPLC analysis.

General experimental procedure for 24 h racemization reactions of enantioenriched 3-chlorobenzoin with different BAs. A dry, argon-flushed 8 ml vial equipped with a magnetic stir bar was charged with Rb_2CO_3 (0.045 mmol) and a 3 Å MS (50 mg) and dried at 200 °C in the oven overnight. The vial was then heated with a heat gun under an argon flow for 5 min and cooled to room temperature. $\mathbf{Cat}_{5F}$ (0.066 mmol) and aryl BA (0.079 mmol) were added and flushed

with argon. The reactions were performed in batches of ten and enantioenriched 3-chlorobenzoin was weighed out to prepare 1.7 g in 11 ml of anhydrous THF, which should amount to 0.55 mmol in each 1 ml. For each batch of reactions, the effective amount (mmol) of 3-chlorobenzoin was determined either by HPLC or NMR using 1,3,5-triisopropylbenzene as the internal standard. 3-chlorobenzoin (1 ml) was added into the reaction vail and the mixture was stirred (500 rpm) at 20 °C for 24 h. The reaction was quenched with distilled acetic acid (30 µL, 0.48 mmol) and stirred for 10 minutes. The solvent was removed under nitrogen flow. To calculate NMR yields a stock solution of 1,3,5-triisopropylbenzene (1 mmol) in $CHCl_3$ (10 mL) was prepared and each reaction mixture was dissolved in 1 mL of the stock solution. An aliquot of the dissolved reaction mixture (200 µL) was used for HPLC enantioenrichment analysis by filtering through silica gel (500 mg) then washing with $CHCl_3$ (5 × 2 mL). After evaporating the solvent, the crude product was dissolved in isopropyl alcohol and the sample was ready for HPLC analysis.

General experimental procedure for crossover experiments. A dry, argon-flushed 8 mL vial equipped with a magnetic stir bar was charged with Rb_2CO_3 (0.045 mmol) and 3 Å MS (50 mg) and dried at 200 °C in the oven overnight. The vial was then heated with a heat gun under an argon flow for 5 min and cooled to room temperature. **Cat**$_{5F}$ (0.066 mmol) and aryl BA (0.099 mmol) were added and flushed with argon. Enantioenriched 3-chlorobenzoin-d (120 mg, 0.42 mmol, in 600 µl of anhydrous THF) and 2-chlorobenzaldehyde (47 µ, 0.42 mmol) were added into the reaction vail and the mixture was stirred (500 r.p.m.) at 20 °C for 24 h. The reaction was quenched with distilled acetic acid (30 µl, 0.48 mmol). An aliquot of the reaction mixture (50 µl) was diluted with 950 µl of acetonitrile, filtered through a 0.45 µm microfilter and used for HPLC product distribution analysis. The rest of the reaction mixture was purified by silica gel column chromatography (EtOAc:hexane 20:80) to determine the enantioenrichment and deuterium incorporation.

General experimental procedure for large-scale reactions. A dry, argon-flushed 25 ml round-bottom flask equipped with a magnetic stir bar was charged with Rb_2CO_3 (0.033 mmol) and a 3 Å MS (30 mg). The flask was then heated with a heat gun under argon flow for 10 min and cooled to room temperature. Cat_{5F} (0.050 mmol) and aryl BA (0.075 mmol) were added, followed by the addition of 3-chlorobenzaldehyde (50 mmol), 15 ml of anhydrous THF and water (30 µl). The reaction mixture was stirred at 20 °C for 20 or 40 h. The reaction was quenched with distilled acetic acid (4.5 ml) and purified by column chromatography (EtOAc:hexane 20:80).

Data availability

All data generated or analysed during this study are available in this published article and its Supplementary Information files, or from the corresponding author upon request. Experimental procedures, results, characterization data, spreadsheets of parameters used in the models and MATLAB scripts used for model identification are accessible online as Supplementary Information.

Received: 22 June 2018; Accepted: 22 March 2019;
Published online: 13 May 2019

References

1. Warren, J. J., Lancaster, K. M., Richards, J. H. & Gray, H. B. Inner- and outer-sphere metal coordination in blue copper proteins. *J. Inorg. Biochem.* **115**, 119–126 (2012).
2. Werner, A. Zur kenntnis des asymmetrischen kobaltatoms. *Ber. Dtschn Chem. Ges.* **45**, 121–130 (1912).
3. Werner, A. Über die raumisomeren kobaltverbindungen. *Justus Liebig's Ann. Chem.* **386**, 1–272 (1912).
4. Cook, S. A. & Borovik, A. S. Molecular designs for controlling the local environments around metal ions. *Acc. Chem. Res.* **48**, 2407–2414 (2015).
5. Reedijk, J. Coordination chemistry beyond Werner: interplay between hydrogen bonding and coordination. *Chem. Soc. Rev.* **42**, 1776–1783 (2013).
6. Shook, R. L. & Borovik, A. S. Role of the secondary coordination sphere in metal-mediated dioxygen activation. *Inorg. Chem.* **49**, 3646–3660 (2010).
7. Baschieri, A., Bernardi, L., Ricci, A., Suresh, S. & Adamo, M. F. Catalytic asymmetric conjugate addition of nitroalkanes to 4-nitro-5-styrylisoxazoles. *Angew. Chem. Int. Ed.* **48**, 9342–9345 (2009).
8. Kawai, H., Kusuda, A., Nakamura, S., Shiro, M. & Shibata, N. Catalytic enantioselective trifluoromethylation of azomethine imines with trimethyl(trifluoromethyl)silane. *Angew. Chem. Int. Ed.* **48**, 6324–6327 (2009).
9. Nicolaou, K. C., Liu, G., Beabout, K., McCurry, M. D. & Shamoo, Y. Asymmetric alkylation of anthrones, enantioselective total synthesis of (−)- and (+)-viridicatumtoxins B and analogues thereof: absolute configuration and potent antibacterial agents. *J. Am. Chem. Soc.* **139**, 3736–3746 (2017).
10. Sahu, S. et al. Secondary coordination sphere influence on the reactivity of nonheme iron(II) complexes: an experimental and DFT approach. *J. Am. Chem. Soc.* **135**, 10590–10593 (2013).
11. Ward, T. R. et al. Exploiting the second coordination sphere: proteins as host for enantioselective catalysis. *Chimia* **57**, 586–588 (2003).
12. Uraguchi, D., Ueki, Y. & Ooi, T. Chiral organic ion pair catalysts assembled through a hydrogen-bonding network. *Science* **326**, 120–123 (2009).
13. Meeuwissen, J. & Reek, J. N. H. Supramolecular catalysis beyond enzyme mimics. *Nat. Chem.* **2**, 615–621 (2010).
14. Leenders, S. H. A. M., Gramage-Doria, R., de Bruin, B. & Reek, J. N. H. Transition metal catalysis in confined spaces. *Chem. Soc. Rev.* **44**, 433–448 (2014).
15. Rowan, S. J., Cantrill, S. J. & Cousins, G. R. L. Dynamic covalent chemistry. *Angew. Chem. Int. Ed.* **41**, 898–952 (2002).
16. Bapat, A. P., Roy, D., Ray, J. G., Savin, D. A. & Sumerlin, B. S. Dynamic-covalent macromolecular stars with boronic ester linkages. *J. Am. Chem. Soc.* **133**, 19832–19838 (2011).
17. Bull, S. D. et al. Exploiting the reversible covalent bonding of boronic acids: recognition, sensing, and assembly. *Acc. Chem. Res.* **46**, 312–326 (2013).
18. Wilson, A., Gasparini, G. & Matile, S. Functional systems with orthogonal dynamic covalent bonds. *Chem. Soc. Rev.* **43**, 1948–1962 (2014).
19. Schaufelberger, F. & Ramström, O. Dynamic covalent organocatalysts discovered from catalytic systems through rapid deconvolution screening. *Chem. Eur. J.* **21**, 12735–12740 (2015).
20. Lascano, S. et al. The third orthogonal dynamic covalent bond. *Chem. Sci.* **7**, 4720–4724 (2016).
21. Seifert, H. M., Ramirez Trejo, K. & Anslyn, E. V. Four simultaneously dynamic covalent reactions. Experimental proof of orthogonality. *J. Am. Chem. Soc* **138**, 10916–10924 (2016).
22. Zhou, Y., Li, L., Ye, H., Zhang, L. & You, L. Quantitative reactivity scales for dynamic covalent and systems chemistry. *J. Am. Chem. Soc.* **138**, 381–389 (2016).
23. Akgun, B. & Hall, D. G. Fast and tight boronate formation for click bioorthogonal conjugation. *Angew. Chem. Int. Ed.* **55**, 3909–3913 (2016).
24. Moulin, E., Cormos, G. & Giuseppone, N. Dynamic combinatorial chemistry as a tool for the design of functional materials and devices. *Chem. Soc. Rev.* **41**, 1031–1049 (2012).
25. Teichert, J. F., Mazunin, D. & Bode, J. W. Chemical sensing of polyols with shapeshifting boronic acids as a self-contained sensor array. *J. Am. Chem. Soc.* **135**, 11314–11321 (2013).
26. Wong, C.-H. & Zimmerman, S. C. Orthogonality in organic, polymer, and supramolecular chemistry: from Merrifield to click chemistry. *Chem. Commun.* **49**, 1679–1695 (2013).
27. Wiskur, S. L. & Anslyn, E. V. Using a synthetic receptor to create an optical-sensing ensemble for a class of analytes: a colorimetric assay for the aging of scotch. *J. Am. Chem. Soc.* **123**, 10109–10110 (2001).
28. Baragwanath, L., Rose, C. A., Zeitler, K. & Connon, S. J. Highly enantioselective benzoin condensation reactions involving a bifunctional protic pentafluorophenyl-substituted triazolium precatalyst. *J. Org. Chem.* **74**, 9214–9217 (2009).
29. O'Toole, S. E. & Connon, S. J. The enantioselective benzoin condensation promoted by chiral triazolium precatalysts: stereochemical control via hydrogen bonding. *Org. Biomol. Chem.* **7**, 3584–3593 (2009).
30. Langdon, S. M., Legault, C. Y. & Gravel, M. Origin of chemoselectivity in N-heterocyclic carbene catalyzed cross-benzoin reactions: DFT and experimental insights. *J. Org. Chem.* **80**, 3597–3610 (2015).
31. Maji, R. & Wheeler, S. E. in *Aromatic interactions: Frontiers in Knowledge and Application* (eds Darren W Johnson, D. W. & Hof, F.) 18–38 (The Royal Society of Chemistry, Cambridge, 2017).
32. Paul, M., Breugst, M., Neudorfl, J. M., Sunoj, R. B. & Berkessel, A. Keto-enol thermodynamics of Breslow intermediates. *J. Am. Chem. Soc.* **138**, 5044–5051 (2016).
33. Flanigan, D. M., Romanov-Michailidis, F., White, N. A. & Rovis, T. Organocatalytic reactions enabled by N-heterocyclic carbenes. *Chem. Rev.* **115**, 9307–9387 (2015).
34. Hansch, C., Leo, A. & Taft, R. W. A survey of Hammett substituent constants and resonance and field parameters. *Chem. Rev.* **91**, 165–195 (1991).
35. Verloop, A., Hoogenstraaten, W. & Tipker, J. in *Drug Design* Vol 7 (ed. Ariens, E. J.) 165–207 (Academic, 1976).
36. Milo, A., Bess, E. N. & Sigman, M. S. Interrogating selectivity in catalysis using molecular vibrations. *Nature* **507**, 210–214 (2014).
37. Glendening, E. D., Landis, C. R. & Weinhold, F. Natural bond orbital methods. *WIREs Comput. Mol. Sci.* **2**, 1–42 (2011).
38. Maji, R. & Wheeler, S. E. Importance of electrostatic effects in the stereoselectivity of NHC-catalyzed kinetic resolutions. *J. Am. Chem. Soc.* **139**, 12441–12449 (2017).
39. Massey, R. S., Collett, C. J., Lindsay, A. G., Smith, A. D. & O'Donoghue, A. C. Proton transfer reactions of triazol-3-ylidenes: kinetic acidities and carbon acid p*K*a values for twenty triazolium salts in aqueous solution. *J. Am. Chem. Soc.* **134**, 20421–20432 (2012).

40. Niu, Y. et al. Experimental and computational gas phase acidities of conjugate acids of triazolylidene carbenes: rationalizing subtle electronic effects. *J. Am. Chem. Soc.* **139**, 14917–14930 (2017).
41. Companyó, X. & Burés, J. Distribution of catalytic species as an indicator to overcome reproducibility problems. *J. Am. Chem. Soc.* **139**, 8432–8435 (2017).
42. Enders, D. & Henseler, A. A direct intermolecular cross-benzoin type reaction: N-heterocyclic carbene-catalyzed coupling of aromatic aldehydes with trifluoromethyl ketones. *Adv. Synth. Catal.* **351**, 1749–1752 (2009).
43. Enders, D. N-heterocyclic carbene catalysed asymmetric cross-benzoin reactions of heteroaromatic aldehydes with trifluoromethyl ketones. *Chem. Commun.* **46**, 6282–6284 (2010).
44. Enders, D., Niemeier, O. & Henseler, A. Organocatalysis by N-heterocyclic carbenes. *Chem. Rev.* **107**, 5606–5655 (2007).
45. Renny, J. S., Tomasevich, L. L., Tallmadge, E. H. & Collum, D. B. Method of continuous variations: applications of Job plots to the study of molecular associations in organometallic chemistry. *Angew. Chem. Int. Ed.* **52**, 11998–12013 (2013).
46. Thordarson, P. Determining association constants from titration experiments in supramolecular chemistry. *Chem. Soc. Rev.* **40**, 1305–1323 (2011).
47. Neel, A. J., Milo, A., Sigman, M. S. & Toste, F. D. Enantiodivergent fluorination of allylic alcohols: data set design reveals structural interplay between achiral directing group and chiral anion. *J. Am. Chem. Soc.* **138**, 3863–3875 (2016).
48. Hall, D. G. *Boronic Acids: Preparation and Applications in Organic Synthesis, Medicine and Materials* 1–133 (Wiley, Weinheim, 2011).
49. Martínez-Aguirre, M. A. & Yatsimirsky, A. K. Brønsted versus Lewis acid type anion recognition by arylboronic acids. *J. Org. Chem.* **80**, 4985–4993 (2015).
50. Collett, C. J. et al. Rate and equilibrium constants for the addition of N-heterocyclic carbenes into benzaldehydes: a remarkable 2-substituent effect. *Angew. Chem. Int. Ed.* **127**, 6991–6996 (2015).

Acknowledgements

This research was supported by the Israel Science Foundation (Grant no. 1193/17). We thank M. Sigman, D. Toste, A. Neel and D. Pappo for fruitful discussions. D.V. acknowledges the PBC for a postdoctoral fellowship. S.C.G. acknowledges the Kreitman Graduate School for a postdoctoral fellowship. Z.A. acknowledges the Kreitman Graduate School for the chemo-tech scholarship. Mass spectra measurements were performed with the help of M. Shema-Mizrachi and M. M. Karpasas.

Author contributions

All the authors designed and performed the experiments and analysed the data. The Supplementary Information was compiled by S.C.G. and D.V., the product distribution by HPLC was performed by Z.A. and mathematical modelling was performed by A.M.

Competing interests

The authors declare no competing interests.

Additional information

Supplementary information is available for this paper at https://doi.org/10.1038/s41557-019-0258-1.

Reprints and permissions information is available at www.nature.com/reprints.

Correspondence and requests for materials should be addressed to A.M.

Publisher's note: Springer Nature remains neutral with regard to jurisdictional claims in published maps and institutional affiliations.